

Journal Pre-proofs

A Multifunctional Eu-based Coordination Polymer Luminescent Sensor for Highly Sensitive and Selective Detection of Fe³⁺ and Acetone

Cheng-Bo Yang, Chun-Bo Jiang, Mu-Yin Zhang, Xue Chen, Ping Zou, Rui-Wu Yang, Han-Bing Rao, Guang-Tu Wang

PII: S0277-5387(19)30661-8
DOI: <https://doi.org/10.1016/j.poly.2019.114216>
Reference: POLY 114216

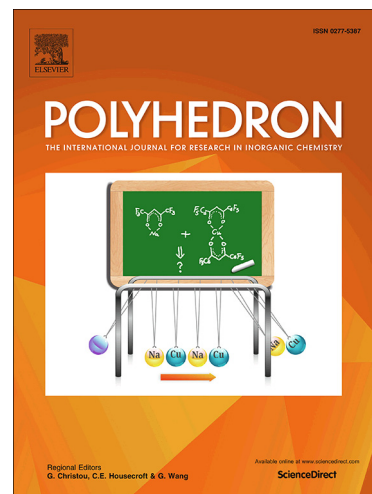
To appear in: *Polyhedron*

Received Date: 19 June 2019
Revised Date: 21 October 2019
Accepted Date: 25 October 2019

Please cite this article as: C-B. Yang, C-B. Jiang, M-Y. Zhang, X. Chen, P. Zou, R-W. Yang, H-B. Rao, G-T. Wang, A Multifunctional Eu-based Coordination Polymer Luminescent Sensor for Highly Sensitive and Selective Detection of Fe³⁺ and Acetone, *Polyhedron* (2019), doi: <https://doi.org/10.1016/j.poly.2019.114216>

This is a PDF file of an article that has undergone enhancements after acceptance, such as the addition of a cover page and metadata, and formatting for readability, but it is not yet the definitive version of record. This version will undergo additional copyediting, typesetting and review before it is published in its final form, but we are providing this version to give early visibility of the article. Please note that, during the production process, errors may be discovered which could affect the content, and all legal disclaimers that apply to the journal pertain.

© 2019 Elsevier Ltd. All rights reserved.



A Multifunctional Eu-based Coordination Polymer Luminescent Sensor for Highly Sensitive and Selective Detection of Fe³⁺ and Acetone

Cheng-Bo Yang,^[a] Chun-Bo Jiang,^[a] Mu-Yin Zhang,^[a] Xue Chen,^[a] Ping Zou,^[a] Rui-Wu Yang,^[b]
Han-Bing Rao,^[a] and Guang-Tu Wang*^[a]

^a College of Science, Sichuan Agriculture University, Ya'an 625014, China

^b College of Life Science, Sichuan Agriculture University, Ya'an 625014, China

Abstract

A new 3D Eu-based coordination polymer, $([\text{Eu}(\text{L})(\text{H}_2\text{O})_3]\text{Cl}\cdot\text{H}_2\text{O})_n$ (**1**) ($\text{H}_2\text{L}=(4\text{-}(\text{pyridyl-N-oxide})\text{methylphosphonic acid})$), was successfully self-assembled via diffusion method at room temperature and characterized by single-crystal X-ray diffraction, elemental analyses, powder X-ray diffraction, thermogravimetric analyses and FT-IR. Single-crystal X-ray diffraction analysis shows that **1** features 3D (4,5)-connected $(3\cdot 4\cdot 5\cdot 6^2\cdot 7)(3^2\cdot 4^2\cdot 5\cdot 6^3\cdot 7^2)$ topological framework with large 1D channels. Photoluminescent spectra of **1** exhibit the strong characteristic luminescence of Eu^{3+} . More importantly, sensing experiments exhibit that **1** can be used as a fluorescence sensor for detecting Fe^{3+} and acetone with excellent sensitivity, great selectivity, reproducibility and low detection limits for Fe^{3+} , and acetone are $0.21\ \mu\text{M}$ and $0.0246\ \text{vol}\%$. It is the first example of Eu-based phosphonate sensor for simultaneous detection of Fe^{3+} and acetone.

Keywords: Coordination Polymer; Luminescence; Sensor; Fe^{3+} ; Acetone

Corresponding author.

E-mail address: gtwang@sicau.edu.cn

Introduction

Coordination polymers (CPs) are among the most active research fields in the design and preparation of novel inorganic-organic hybrid materials,^[1] which are widely used in the areas of catalysis^[2], gas storage and separation^[3], bioimaging^[4], proton conduction^[5], magnetism^[6] and fluorescence^[7]. So far, a large number of fluorescent CPs with infinite three-dimensional structures have been successfully self-assembled^[8], by rationally designed ligands as linkers and carefully selected metal ions as nodes.^[9] For example, Liu et al. used transition metal $[\text{Zn}(\text{ClO}_4)_2 \cdot 6\text{H}_2\text{O}]$, 2,2'-bipyridine and 3-(3',5'-dicarboxylphenoxy)phthalic acid to form Zn-coordination polymer material with strong photoluminescence by hydrothermal reaction.^[10] Compared with the transition metal CPs, lanthanide metals feature excellent inherent photoluminescence features, i.e., the narrow emission peak, large Stokes shift, long fluorescence lifetime and pure chromaticity.^[11] Thus, the design, synthesis and characterization of luminescent lanthanide CPs (Ln-CPs) are one of the fastest-growing fields in material research today.^[12] Particularly, they are used to detect different types of analytes, including small organic molecules^[13], metal cations^[14], anions^[15] and explosives^[16].

Ferric ions, widely found in environmental and biological systems, play crucial roles in almost all types of biosystems like cell metabolism, synthesis of DNA and RNA. However, Fe^{3+} level above and below the normal allowable limits can cause serious illness. Acetone is one of the most common organic solvents used in the laboratory and industrial production^[17]. It is flammable, toxic, explosive and harmful to the environment^[14a,18]. Conventional methods of detecting Fe^{3+} and acetone include spectrophotometry, atomic absorption spectroscopy, ion mobility spectroscopy, inductively coupled plasma atomic emission spectroscopy, electrochemical methods gas chromatography and mass spectrometry. However, these methods sometimes mainly require complicated pre-processing and expensive instruments.^[13a, 14b, 17a, 19] In contrast, Ln-CPs fluorescence sensors are convenient and economical in detect-

ing Fe^{3+} and acetone. Not long ago, Ma et al. reported a luminescent Tb-CPs which can be used as a multifunctional probe to simultaneously sense Fe^{3+} and acetone.^[1f] Despite a variety of Ln-CPs sensors reported to date, more efforts were focused on the lanthanide carboxylic acid complexes.^[18b, 20] Lanthanide phosphonate sensors are rarely developed.^[21] Compared with carboxylates, phosphonates form stronger bonds with metal atoms, which exhibit higher thermal and chemical stabilities.^[20b] Moreover, phosphonate groups have more coordination centers, which can yield rich structural diversities and fascinating luminescent properties.^[21c] To the best of our knowledge, lanthanide phosphonates have not been explored as multifunctional sensors for the detection of Fe^{3+} and acetone. So, it is of significance to study the synthesis, structure, properties and sensing applications of lanthanide phosphonates.

In previous work, we reported series of lanthanide phosphonates constructed by 2-(pyridyl-N-oxide)methylphosphonic acid ligand. Among them, $[\text{Eu}(\text{HL})((\text{C}_2\text{O}_4)_{0.5})_2(\text{H}_2\text{O})]\cdot 3\text{H}_2\text{O}$ have been confirmed to have excellent photoluminescence properties.^[22] However, the construction of an infinite 3D network requires a second ligand assist. Speculatively, this may be because the phosphonate group and the pyridyl group of the ortho-phosphonate ligand are closer, hindering the further growth of the complex in three dimensions. With the further increase of the distance between pyridine and phosphonate, the components may construct a 3D network without the second ligand, and 4-(pyridyl-N-oxide)methylphosphonic acid (H_2L) could be designed and synthesized (Scheme 1). Fortunately, H_2L and Eu^{3+} form a new type of Eu-based lanthanide coordination polymer at room temperature (just using one tube). Structural analysis reveals the complex displays (4,5) two-node 3D network with 1D channels, the point symbol of $(3\cdot 4\cdot 5\cdot 6^2\cdot 7)$ ($3^2\cdot 4^2\cdot 5\cdot 6^3\cdot 7^2$). The solid-state luminescence behavior of **1** indicates that H_2L can effectively sensitize Eu^{3+} characteristic red luminescence. Further studies of the sensing behavior of **1** show that **1** can detect Fe^{3+} and acetone by fluorescence emission and quenching, and has high K_{sv} values and low detection limits for Fe^{3+} and

acetone.

Experimental Section

Materials and methods

All chemicals and reagents are commercially available as reagent grades and are used without further purification. FT-IR spectra were carried out in the range of 4000-500 cm^{-1} using DGTS detector (32 scans) by using KBr disks. Elemental analysis data of C, H, N was collected with an Elementar Vario ELIII analyzer. ^1H NMR spectra were measured using a DRX-400 MHz (Bruker) superconducting-magnet NMR spectrometer. Thermal analyses were conducted on a Perkin-Elmer STA 6000 with a heating rate of 10 $^{\circ}\text{C}/\text{min}$ at the temperature ranging from 40 to 650 $^{\circ}\text{C}$ under air. Powder X-ray diffraction patterns (PXRD) were carried out on a D/MAX-3C X-ray diffractometer using $\text{Cu K}\alpha$ radiation with 2θ range of 5-50 $^{\circ}$ and scanning rate of 0.02 $^{\circ}/\text{s}$ (2θ) at room temperature. UV-vis absorption spectra are measured with an Agilent 8453 spectrometer. The luminescent excitation/emission spectra of the powdered solid samples were recorded at room temperature on an Edinburgh FL920. The absolute external luminescent quantum yield and fluorescence lifetime were determined using an integrating sphere equipped on an Edinburgh FLS 920 phosphorimetry. Adsorption data was collected on outgassed samples (160 $^{\circ}\text{C}$ for 12 h) on a Micromeritics ASAP 2460 gas adsorption analyzer.

Synthesis of 4-chloromethylpyridine(I).

Firstly, a sample of 4-chloromethylpyridine hydrochloride (5.00 g, 30.48 mmol) was dissolved in water (15 mL), and dichloromethane (25 mL) was added under stirring conditions. Then, saturated aqueous NaHCO_3 solution was added dropwise to give a pH=8 solution. After a while, the phases were separated, and the organic compounds were extracted with dichloromethane (6×30 mL). Finally, the

organic layers were combined and dried with anhydrous magnesium sulfate before the solvent was removed.

Synthesis of (4-pyridylmethyl) diethyl phosphate(II).

Diethyl phosphite (8 mL, 62.19 mmol) and sodium (1.2 g, 52.19 mmol) were added to a toluene (30 mL) under nitrogen. Then, 4-chloromethylpyridine (I) in toluene (15 mL) was added to the mixture at room temperature. The resulting suspension was stirred in the dark for 24 hours. After that, the organic compounds were extracted with ethyl acetate (4 × 20 mL). The organic layers were combined and concentrated. The light yellow oil (6.46 g, 28.20 mmol) was purified by flash chromatography on silica gel (PE:EA (4:1 V/V)). Yield: 92.50%. ¹H NMR (400 MHz, CDCl₃) δ = 8.48-8.03 (m, 2H), 7.08 (d, *J*=28.1, 2H), 4.08-3.69 (m, 4H), 2.99 (ddd, *J*=28.3, 15.6, 12.3, 2H), 1.22-0.85 (m, 6H).

Synthesis of 4-((diethoxyphosphoryl)methyl)pyridine-1-oxide(III).

m-CPBA (7.8 g, 33.90 mmol) and II (6.46 g, 28.20 mmol) in DCM (50 mL) were stirred at room temperature overnight, then the solvent was evaporated under vacuum. Purification of the residue was achieved using flash chromatography (PE:EA (2:1 V/V)) to give the oily liquid (5.88 g, 23.99 mmol). Yield: 85.07%. ¹H NMR (400 MHz, CDCl₃) δ = 8.11 (d, *J*=6.0, 2H), 7.22-7.14 (m, 2H), 4.02 (dq, *J*=14.3, 7.1, 4H), 3.10 (s, 1H), 3.04 (s, 1H), 1.27-1.15 (m, 6H).

Synthesis of 4-(pyridyl-N-oxide)methylphosphonic acid (H₂L).

III (4-((diethoxyphosphoryl)methyl)pyridine-1-oxide) (5.88 g, 23.99 mmol) in HCl (25 mL, 18%) was stirred at 90 °C for 24 h. The resulting solution was concentrated under reduced pressure to give oil. Then, the oil in acetone (50 mL) was stirred vigorously at room temperature and a white powder solid

was formed. Finally, the filtrate was removed by filtration, and the white solid was dried under vacuum (3.40 g, 17.97 mmol). Yield: 74.89%. Mp: 147.7-148.5 °C. ^1H NMR (400 MHz, D_2O) δ = 8.31 (dd, $J=11.8, 5.5, 2\text{H}$), 7.61-7.34 (m, 2H), 3.21-2.96 (m, 2H).

Synthesis of $([\text{Eu}(\text{L})(\text{H}_2\text{O})_3]\text{Cl}\cdot\text{H}_2\text{O})_n$ (**1**).

The aqueous solutions of H_2L (1 mL, 0.10 mmol) and $\text{EuCl}_3\cdot 6\text{H}_2\text{O}$ (0.5 mL, 0.10 mmol) were placed in a test tube, and then acetonitrile was diffused into the mixture. Thereafter, the test tube was sealed and stored for 15 days at room temperature. Colorless crystals of **1** were obtained in 49.51% yield (based on Eu). Elemental analysis (%) Calcd for **1** ($\text{C}_6\text{H}_{14}\text{ClNO}_8\text{PEu}$: 446.56): C, 16.12%; H, 3.14%; N, 3.14%. Found: C, 16.19% ; H, 3.11% ; N, 3.11% . IR (KBr, cm^{-1}): 3440s, 1647s, 1490s, 1450m, 1423m, 1236vs, 1215s, 1195s, 1151m, 1115m, 1053m, 997m, 850v, 790m, 702vs, 601v, 547vs, 503s.

X-ray Crystallography.

The diffraction data of the complex was collected through a Bruker APEX-II CCD with graphite monochromated Mo $\text{K}\alpha$ radiation ($\lambda = 0.71073 \text{ \AA}$). Empirical absorption corrections were operated using the SADABS program. The structure was solved and the refined by the direct method and full-Matrix least-squares method on F^2 , respectively ^[23]. All non-hydrogen atoms were refined with anisotropic thermal parameters. And hydrogen atoms attached to the carbon atoms were placed in the calculation position and refined using a ride model.

Results and Discussion

Crystal structure description

Single-crystal X-ray diffraction analysis reveals that the **1** crystallizes in the monoclinic system with the $P12_1/c1$ space group. As shown in Fig. 1a, the asymmetric unit of **1** consists of one crystallographically independent Eu^{3+} ion, one L^{2-} , three coordinating water molecules and one lattice water molecule and one chloride ion. The unique Eu^{3+} ion is eight-coordinated in a Snub diphendoid J84 geometry defined by five oxygen atoms (O1C, O2B, O3B, O3A, O4) from four L^{2-} , and the remaining three coordination sites are occupied by three oxygen atoms from the coordinating water molecule (Figure S1).^[24] O4 and O3A are derived from the phosphonate of two ligands, respectively. O2B and O3B are derived from a phosphonate of L^{2-} . O1C is derived from the N-O oxides of the L^{2-} . O5W, O6W, and O7W are from three coordinating water molecules. Similar to other reported Eu complexes based on phosphonate ligands,^[25] the bond distances between Eu-O (L^{2-}) are 2.318(3) and 2.678(3) Å with the average bond length of 2.414 Å. Moreover, the crystallographic and structural data of **1** are summarized in Table S1-S2.

In the complex **1**, the neighbouring Eu^{3+} ions are connected by ligand phosphate groups to produce a chain structure with an infinite corrugated shape along the a-axis. The distance between $\text{Eu}\cdots\text{Eu}$ is 4.1782(5) Å and 5.4344(4)Å, respectively. Eu-O-Eu angle is 112.60° (Fig 1b). Each chain is further bonded to one another by ligands to form a three-dimensional framework with 1D channels along the a-axis direction (Fig 1c). The L^{2-} acts as a four-coordination linker, coordinating to four Eu^{3+} via its three phosphonate oxygen atoms and one pyridine N-O oxygen atom with bridging and coupling modes, wherein the phosphate group is coordinated to three Eu^{3+} ions; nitrogen oxide pyridine oxygen atom is

linked to a Eu^{3+} ion (Fig S2). Furthermore, the porosity of the **1** was calculated by PLATON to be 20%, after removing the lattice water molecules and Cl^{-} [26].

To simplify the three-dimensional structure of complex **1**, a topological analysis was executed. Eu^{3+} and L^{2-} can be regarded as five- and four-coordinated node, respectively. Thence this framework could be simplified as a 3D (4,5)-connected bimodal topological structure with the Schläfli symbol as $(3\cdot4\cdot5\cdot6^2\cdot7)$ and $(3^2\cdot4^2\cdot5\cdot6^3\cdot7^2)$ calculated by the TOPOS program[27] (Fig. 1d).

Thermogravimetric analysis (TGA) and powder X-ray diffraction (PXRD)

In order to investigate the phase purity and the stability of the entire skeleton of complex **1**, powder X-ray diffraction (PXRD) and thermogravimetric (TG) measurements were carried out. The PXRD pattern for **1** is presented in Fig.S3. The diffraction peaks of both simulated and experiment patterns are in good agreement with each other, indicating the phase purities of **1**.

The thermal stability test of complex **1** was performed under air conditions at the temperatures ranging from 40 to 650 °C (Fig. S4). The initial weight loss of 15.7% corresponds to the loss of four water molecule (one solvent water molecule and three coordinating water molecules) during 40-250 °C (calcd. 16.1%). Further heating to 400 °C shows little loss of weight, indicating the dehydrated framework of **1** is thermally stable over this temperature range. Finally, the residue weight is 69.4%, probably due to the formation of a mixture of Eu_2O_3 and EuPO_4 in a molar ratio of 1:1 (calcd. 67.1%).

Photoluminescence properties

The solid-state excitation and emission spectra of complex **1** have been measured at ambient temperature (Fig. 2). The emission spectrum of **1** shows photoluminescence with four typical Eu^{3+} emission peaks at 592 nm, 612 nm, 651 nm, and 701 nm ($\lambda_{\text{ex}}=293$ nm) due to the $^5\text{D}_0 \rightarrow ^7\text{F}_j$ ($j=1, 2, 3$ and 4) transition originating from antenna effects. The most intense emission peak is located at 612 nm, corre-

spending to the ${}^5D_0 \rightarrow {}^7F_2$ transition [28]. The fluorescence lifetime of **1** is 2.36 ms, which is in line with the single exponential curve. The fluorescence quantum yield of this complex is 9.3%.

Sensing of Fe^{3+}

In order to study the potential of complex **1** for the sensing of metal cations, the finely ground powder sample of **1** (4mg) was dispersed in a series of DMF (4mL) solutions containing $M(NO_3)_X$ (concentration = 1mM; $M^{X+} = Na^+, Ca^{2+}, Ag^+, Ni^{2+}, Pb^{2+}, Mg^{2+}, Ba^{2+}, Cd^{2+}, Al^{3+}, K^+, Zn^{2+}, Cr^{3+}, Co^{2+}, Cu^{2+}, Fe^{3+}$; since Fe^{2+} can be easily oxidized to Fe^{3+} , the influence of Fe^{2+} is not discussed herein), then treated with ultrasonication for 30 min, and aged for 12 h to form a stable suspension. Finally, the ultrasonication was performed for 30 min before the fluorescence detection. The fluorescence results show that the fluorescence intensity of **1** is almost completely quenched in the Fe^{3+} nitrate solution, while other metal ions have no such significant effect (Fig. 3). This phenomenon implies that **1** can sense Fe^{3+} selectively. Moreover, when **1**, Fe^{3+} and other various metal ions (including the same concentration of Fe^{3+}) exist simultaneously, the fluorescence intensity of **1** is also significantly quenched (Fig. S7a). The results indicate that the fluorescence quenching effect of **1** is not inhibited by other metal ions while detecting Fe^{3+} . That is, the anti-interference ability of **1** is strong.

To further study the detection limit of complex **1** for Fe^{3+} , the fluorescence intensity of **1** in the presence of different concentrations of Fe^{3+} was measured using a fluorescence titration method. As shown in Fig. 4a, as the concentration of Fe^{3+} increases from 0 to 2.5×10^{-4} M, the fluorescence intensity of **1** decreases continuously. The detection limit reaches 5×10^{-6} M; the quenching effect of Fe^{3+} reaches 14.5% (The quenching effect is defined by $(I_0 - I)/I_0 \times 100\%$, where I_0 and I refer to the fluorescence intensity of **1** before and after the addition of Fe^{3+} , respectively^[14c]). When the Fe^{3+} concentration is 2.5×10^{-4} M, the quenching effect reaches 83.4%. The fluorescence quenching effect of Fe^{3+} on **1** was

further evaluated using the Stern-Volmer formula $I_0/I = 1 + K_{sv} \times [Q]$ [29] (I_0 and I refer to the fluorescence intensity of **1** at 612 nm before and after the addition of Fe^{3+} , $[Q]$ refers to the concentration of Fe^{3+} , and K_{sv} is the fluorescence quenching constant). The Stern-Volmer plot (Figure 4b) shows a good linear correlation between the fluorescence intensity of **1** and the concentration of Fe^{3+} at low concentrations ($R^2 = 0.9961$): the K_{sv} is estimated to be $1.2549 \times 10^4 M^{-1}$, and the detection limit is calculated to be $0.21 \mu M$. The K_{sv} value of **1** is comparable to those reported in the previous literature (Table S3) [30].

Sensing of Acetone molecules

Inspired by the complex **1** sensing behavior of Fe^{3+} , the sensing ability of **1** for different small organic molecules is further explored. Similar to the previous **1** for Fe^{3+} sensing, the powder sample of **1** (4 mg) was added to 4 mL various organic small molecules (methanol, ethanol, DMF, acetonitrile, ethyl acetate, methyl tert-butyl ether, DCM, chloroform, THF, dioxane, cyclohexane and acetone). After that, the mixture was treated by ultrasonication for 30 min and then aged for 12 h to form a stable suspension. The results show that (Fig. 5), acetone can completely quench the emission of **1**, indicating that **1** can be used as a fluorescent sensor for acetone. Of course, the **1** has also been studied the ability to selectively detect acetone. When **1**, acetone and other small organic molecules (the same volume of each small organic molecule) are present simultaneously, the fluorescence intensity of **1** is also quenched (Fig. S7b). It indicates that **1** has good anti-interference ability for other organic small molecules in sensing acetone.

The detection limit of complex **1** for acetone is also explored. In Fig. 6, the fluorescence emission intensity of **1** decreases with the increased volume fraction of acetone (0-4.8%): the detection limit is 0.1% and the quenching effect reaches 12.7%. When the volume fraction of acetone reaches 4.8%, the quenching effect achieves 98.1%. Further testing the acetone detection limit using the Stern-Volmer

formula with a linear correlation of $R^2 = 0.9855$ at low concentrations, the K_{sv} reaches 1.25 and the detection limit is calculated to be 0.0246 vol% (Table S3) [31].

Regeneration performance

It is well known that the recyclability of sensing materials is one important parameter in evaluating the usability of a sensor. Therefore, the regeneration performance of **1** for the detection of Fe^{3+} and acetone are also investigated. As shown in Fig. 7, after **1** sensed Fe^{3+} and acetone, the samples were simply washed several times with DMF to remove residual Fe^{3+} and acetone, and then recovered by centrifugation. The fluorescence detection results show that the fluorescence intensity of **1** can be recovered substantially at least 5 times for the detection of Fe^{3+} and acetone. It can be seen from the PXRD pattern that the crystal structure of **1** does not collapse significantly after five cycles of detection of Fe^{3+} and acetone.

Interestingly, the characteristic diffraction peaks of **1**@ Fe^{3+} , **1**(5)@ Fe^{3+} and **1**(5)@Acetone are slightly shifted from **1**, while the diffraction peaks of **1**@Acetone fit well with **1** (Fig.S3). Therefore, the PXRD of **1**@DMF is collected to verify if DMF causes these shifts. The results show that the PXRD of **1**@DMF can be fitted with **1**@ Fe^{3+} , **1**(5)@ Fe^{3+} and **1**(5)@Acetone diffraction peaks. In other words, DMF causes these PXRD diffraction peak shifts. If DMF is removed, the shift of this PXRD characteristic diffraction peak may be restored. As expected, the diffraction peaks shift of **1**@ Fe^{3+} after washing with an acetonitrile/ H_2O (V/V:5/1) mixed solvent was recovered. This phenomenon further indicates that the displacement of the characteristic diffraction peak of PXRD may be caused by DMF solvent molecules (Fig.S3).

Mechanism of fluorescence sensing

In prior literature data, the generation of fluorescence quenching for **1** may come from the following aspects: (i) the collapse of crystal structure;^[32] (ii) the absorption and/or excitation spectra of **1** overlap with absorption spectra of analytes;^[1f, 19c] (iii) the exchange of central metal ions of **1** and target cations inter-ion;^[33] (iv) the interaction between metal cations and organic ligands.^[34]

Firstly, the PXRD patterns of **1**@Fe³⁺ and **1**@DMF show that the PXRD patterns of the two fits well (Fig. S3), indicating that the crystal structure of **1** does not change before and after Fe³⁺ treatment. Therefore, the crystal structure collapse is first excluded. Secondly, in the Fe³⁺ limit detection experiment, it is found that the Fe³⁺ concentration increased slightly, and the fluorescence intensity of **1** decreased slightly in a short time, suggesting that **1** has a fast response to Fe³⁺, thus excluding ion exchange between central metal ions of **1** and target cations. Simultaneously, the fluorescence performance of **1** after simple cleaning with DMF restored, and it also suggests that cation exchange is not the fluorescence quenching mechanism of **1** sensing Fe³⁺.

Thirdly, it is found by UV-visible absorption experiments that the absorption spectrum of Fe³⁺ has a large coverage with the excitation spectrum of **1** (Fig. S5a), while other metal ions have no large coverage. This phenomenon indicates that competition for energy absorption by **1** and Fe³⁺ is one of the reasons for **1** fluorescence quenching.

Fourthly, for **1** before and after treatment with Fe³⁺, the O1s peak in the XPS spectrum is designated as O in the ligand pyridine oxynitride and phosphonate groups, and the N1s peak is designated as the ligand pyridine ring (Fig.S6). The N1s peak changes from 403.1 eV to 402.5 eV and the O1s peak changes from 531.4 eV to 531.8 eV, due to the weak interaction of N and O atom in Fe³⁺ and **1**. Therefore, there is a weak interaction between Fe³⁺ and the ligand of **1**, and the energy absorbed by the ligand is partially transferred to Fe³⁺, which also causes a decrease in fluorescence intensity.

For acetone, the mechanism of fluorescence quenching that occurring through previous literatures show that effective sense acetone based on **1** is often attributed to energy absorption competition^[1g, 21c, 35]. Therefore, we first tested the PXRD pattern of acetone-treated **1** and found that it can be well fitted, which proves that the crystal structure of **1** does not collapse, excluding the reason of crystal structure damage.

After the UV absorption test of each organic solvent, it is found that the absorption spectrum of acetone and the excitation spectrum of **1** were greatly covered, while other organic small molecules were weaker than acetone (Fig. S5b). It is obvious that the energy absorption of **1** and acetone is the main reason for the quenching of **1**.

These phenomena indicate that the **1** can be used as potential fluorescent sensors for Fe³⁺ and acetone, with high sensitivity, high selectivity and regenerability.

Conclusions

In summary, a new coordination polymer ([Eu(L)(H₂O)₃]Cl·H₂O)_n was successfully self-assembled by 4-(pyridyl-N-oxide)methylphosphonic acid (H₂L) ligand via using diffusion method at room temperature. **1** displays a three-dimensional network structure with 1D channels, presenting a (4,5)-connected topological framework with a point symbol of (3·4·5·6²·7) (3²·4²·5·6³·7²). The luminescence sensing experiments of **1** demonstrate excellent selectivity and high sensitivity for the detection of Fe³⁺ and acetone, and the detection limits for Fe³⁺ and acetone are 0.21 μM and 0.0246 vol%, respectively. In addition, the sensor can be easily and quickly regenerated, indicating good recyclability for the detection of Fe³⁺ and acetone. These properties indicate that the **1** functional material has great potential for detecting acetone and Fe³⁺.

Acknowledgments

This work was supported by Two-Way Support Programs of Sichuan Agricultural University (Nos. 03572832 and 03572227).

Appendix A. Supplementary data

CCDC 1872143 contains the supplementary crystallographic data for complex **1**. These data can be obtained free of charge via <http://www.ccdc.cam.ac.uk/conts/retrieving.html>, or from the Cambridge Crystallographic Data Centre, 12 Union Road, Cambridge CB2 1EZ, UK; fax: (+44) 1223-336-033; or e-mail: deposit@ccdc.cam.ac.uk.

References

- [1] a) S. M. F. Vilela, R. F. Mendes, P. Silva, J. A. Fernandes, J. P. C. Tomé, F. A. A. Paz, *Crystal Growth & Design* **2013**, *13*, 543-560; b) Y. Z. Zheng, M. Evangelisti, F. Tuna, R. E. Winpenny, *J Am Chem Soc* **2012**, *134*, 1057-1065; c) M. Starck, R. Ziessel, *Dalton transactions* **2012**, *41*, 13298-13307; d) L. Y. Guo, H. F. Su, M. Kurmoo, X. P. Wang, Q. Q. Zhao, S. C. Lin, C. H. Tung, D. Sun, L. S. Zheng, *ACS applied materials & interfaces* **2017**, *9*, 19980-19987; e) W. M. Chen, X. L. Meng, G. L. Zhuang, Z. Wang, M. Kurmoo, Q. Q. Zhao, X. P. Wang, B. Shan, C.-H. Tung, D. Sun, *Journal of Materials Chemistry A* **2017**, *5*, 13079-13085; f) X. Han, J. Yang, Y.Y. Liu, J.F. Ma, *Dyes and Pigments* **2019**, *160*, 492-500; g) X. Dao, Y. Ni, H. Pan, *Sensors and Actuators B: Chemical* **2018**, *271*, 33-43.
- [2] a) H. Yang, X. Zhang, G. Zhang, H. Fei, *Chemical communications* **2018**, *54*, 4469-4472. b) Q. Gao, J. Xu, X. H. Bu, *Coordination Chemistry Reviews* **2019**, *378*, 17-31; c) N. Maksimchuk, M. Timofeeva, M. Melgunov, A. Shmakov, Y. Chesalov, D. Dybtsev, V. Fedin, O. Kholdeeva, *Journal of Catalysis* **2008**, *257*, 315-323; d) T. Ishida, M. Nagaoka, T. Akita, M. Haruta, *Chemistry* **2008**, *14*, 8456-8460.
- [3] a) X. Y. Li, L. N. Ma, Y. Liu, L. Hou, Y. Y. Wang, Z. Zhu, *ACS applied materials & interfaces* **2018**, *10*,

- 10965-10973; b) M. Zhang, W. Zhou, T. Pham, K. A. Forrest, W. Liu, Y. He, H. Wu, T. Yildirim, B. Chen, B. Space, *Angewandte Chemie* **2017**, *129*, 11584-11588; c) J. Lu, C. Perez-Krap, M. Suyetin, N. H. Alsmail, Y. Yan, S. Yang, W. Lewis, E. Bichoutskaia, C. C. Tang, A. J. Blake, R. Cao, M. Schroder, *J Am Chem Soc* **2014**, *136*, 12828-12831; d) N. H. Alsmail, M. Suyetin, Y. Yan, R. Cabot, C. P. Krap, J. Lu, T. L. Easun, E. Bichoutskaia, W. Lewis, A. J. Blake, M. Schroder, *Chemistry* **2014**, *20*, 7317-7324; e) J. Jia, X. Lin, A. J. Blake, N. R. Champness, P. Hubberstey, L. Shao, G. Walker, C. Wilson, M. Schroder, *Inorganic chemistry* **2006**, *45*, 8838-8840; f) J. X. Ma, X. F. Huang, X. Q. Song, W. S. Liu, *Chemistry* **2013**, *19*, 3590-3595; g) J. B. Lin, J. P. Zhang, X. M. Chen, *J Am Chem Soc* **2010**, *132*, 6654-6656.
- [4] a) X. P. Yang, S. Q. Wang, Y. Zhang, G. Liang, T. Zhu, L. j. Zhang, S. M. Huang, D. Schipper, R. A. Jones, *Chemical science* **2018**, *9*, 4630-4637; b) D. Liu, R. C. Huxford, W. Lin, *Angewandte Chemie* **2011**, *50*, 3696-3700.
- [5] Z. Hassanzadeh Fard, N. E. Wong, C. D. Malliakas, P. Ramaswamy, J. M. Taylor, K. Otsubo, G. K. H. Shimizu, *Chemistry of Materials* **2018**, *30*, 314-318; b) M. Zhu, L. Han, Q.-Q. Wang, M.-J. Wei, T. Su, C.-Y. Sun, X.-L. Wang, Z.-M. Su, *Inorganic Chemistry Communications* **2018**, *96*, 153-158.
- [6] a) B. S. Dolinar, D. I. Alexandropoulos, K. R. Vignesh, T. James, K. R. Dunbar, *J Am Chem Soc* **2018**, *140*, 908-911; b) J. S. Feng, M. Ren, Z. S. Cai, K. Fan, S. S. Bao, L. M. Zheng, *Chemical communications* **2016**, *52*, 6877-6880; c) J. S. Feng, S. S. Bao, M. Ren, Z. S. Cai, L. M. Zheng, *Chemistry* **2015**, *21*, 17336-17343; d) Y. X. Ren, X. J. Zheng, L. C. Li, D. Q. Yuan, M. An, L. P. Jin, *Inorganic chemistry* **2014**, *53*, 12234-12236; e) P. Mondal, B. Dey, S. Roy, S. P. Bera, R. Nasani, A. Santra, S. Konar, *Crystal Growth & Design* **2018**, *18*, 6211-6220.
- [7] a) C. Wei, B. Sun, Z. Cai, Z. Zhao, Y. Tan, W. Yan, H. Wei, Z. Liu, Z. Bian, C. Huang, *Inorganic chemistry* **2018**, *57*, 7512-7515; b) T. C. Jenks, M. D. Bailey, B. A. Corbin, A. N. W. Kuda-Wedagedara, P. D. Martin, H. B. Schlegel, F. A. Rabuffetti, M. J. Allen, *Chemical communications* **2018**, *54*, 4545-4548; c) T. Y. Bing, T. Kawai, J. Yuasa, *J Am Chem Soc* **2018**, *140*, 3683-3689; d) H. Zhang, L. Zhou, J. Wei, Z. Li, P. Lin, S. Du, *Journal of Materials Chemistry* **2012**, *22*, 21210. e) D. Tian, X. J. Liu, R. Feng, J. L. Xu, J. Xu, R. Y. Chen, L. Huang, X. H. Bu, *ACS*

- applied materials & interfaces* **2018**, *10*, 5618-5625; f) D. Das, K. Biradha, *Crystal Growth & Design* **2018**, *18*, 3683-3692.
- [8] a) M. J. Białek, J. Janczak, J. Zoń, *CrystEngComm* **2013**, *15*, 390-399; b) R. M. P. Colodrero, K. E. Papathanasiou, N. Stavgianoudaki, P. Olivera-Pastor, E. R. Losilla, M. A. G. Aranda, L. León-Reina, J. Sanz, I. Sobrados, D. Choquesillo-Lazarte, J. M. García-Ruiz, P. Atienzar, F. Rey, K. D. Demadis, A. Cabeza, *Chemistry of Materials* **2012**, *24*, 3780-3792; c) M. Inukai, M. Tamura, S. Horike, M. Higuchi, S. Kitagawa, K. Nakamura, *Angewandte Chemie* **2018**, *57*, 8687-8690.
- [9] a) Y. Y. Zhu, Z. G. Sun, F. Tong, Z. M. Liu, C. Y. Huang, W. N. Wang, C. Q. Jiao, C. L. Wang, C. Li, K. Chen, *Dalton transactions* **2011**, *40*, 5584-5590; b) J. Rocha, F. A. Almeida Paz, F.-N. Shi, D. Ananias, N. J. O. Silva, L. D. Carlos, T. Trindade, *European Journal of Inorganic Chemistry* **2011**, *2011*, 2035-2044; c) T. H. Zhou, F. Y. Yi, P. X. Li, J. G. Mao, *Inorganic chemistry* **2010**, *49*, 905-915; d) Y. Zhu, Z. Sun, Y. Zhao, J. Zhang, X. Lu, N. Zhang, L. Liu, F. Tong, *New J. Chem.* **2009**, *33*, 119-124; e) Z. Q. Yao, G. Y. Li, J. Xu, T. L. Hu, X. H. Bu, *Chemistry* **2018**, *24*, 3192-3198; f) C. X. Wang, Y. P. Xia, Z. Q. Yao, J. Xu, Z. Chang, X. H. Bu, *Dalton transactions* **2019**, *48*, 387-394; g) Y. Q. Zhang, V. A. Blatov, T. R. Zheng, C. H. Yang, L. L. Qian, K. Li, B. L. Li, B. Wu, *Dalton transactions* **2018**, *47*, 6189-6198.
- [10] L.N. Wang, Y.H. Zhang, S. Jiang, Z.Z. Liu, *CrystEngComm* **2019**, *21*, 4557-4567.
- [11] a) K. Chen, D. P. Dong, Z. G. Sun, C. Q. Jiao, C. Li, C. L. Wang, Y. Y. Zhu, Y. Zhao, J. Zhu, S. H. Sun, M. J. Zheng, H. Tian, W. Chu, *Dalton transactions* **2012**, *41*, 10948-10956; b) Z. Amghouz, J. R. García, S. García-Granda, A. Clearfield, J. Rodríguez Fernández, I. de Pedro, J. A. Blanco, *Journal of Alloys and Compounds* **2012**, *536*, S499-S503; c) X. Hu, W. Dou, C. Xu, X. Tang, J. Zheng, W. Liu, *Dalton transactions* **2011**, *40*, 3412-3418; d) D.-P. Dong, L. Liu, Z.-G. Sun, C.-Q. Jiao, Z.-M. Liu, C. Li, Y.-Y. Zhu, K. Chen, C.-L. Wang, *Crystal Growth & Design* **2011**, *11*, 5346-5354.
- [12] a) L. Liu, Z. G. Sun, N. Zhang, Y. Y. Zhu, Y. Zhao, X. Lu, F. Tong, W.-N. Wang, C.-Y. Huang, *Crystal Growth &*

- Design* **2010**, *10*, 406-413; b) S. Lis, G. Pawlicki, *Journal of Luminescence* **2010**, *130*, 832-838; c) X. Li, T. Liu, Q. Lin, R. Cao, *Crystal Growth & Design* **2010**, *10*, 608-617; d) J. Troyano, Ó. Castillo, P. Amo-Ochoa, J. I. Martínez, F. Zamora, S. Delgado, *CrystEngComm* **2019**, *21*, 3232-3239; e) J. Y. Ge, Z. Chen, L. Zhang, X. Liang, J. Su, M. Kurmoo, J. L. Zuo, *Angewandte Chemie* **2019**, *58*, 8789-8793.
- [13] a) W. Yan, C. Zhang, S. Chen, L. Han, H. Zheng, *ACS applied materials & interfaces* **2017**, *9*, 1629-1634; b) M.-L. Han, G.-X. Wen, W.-W. Dong, Z.-H. Zhou, Y.-P. Wu, J. Zhao, D.-S. Li, L.-F. Ma, X. Bu, *Journal of Materials Chemistry C* **2017**, *5*, 8469-8474; c) Z. Tang, H. Chen, Y. Zhang, B. Zheng, S. Zhang, P. Cheng, *Crystal Growth & Design* **2019**, *19*, 1172-1182.
- [14] a) Q. Zhang, J. Wang, A. M. Kirillov, W. Dou, C. Xu, C. Xu, L. Yang, R. Fang, W. Liu, *ACS applied materials & interfaces* **2018**, *10*, 23976-23986; b) H. Zhang, R. Fan, W. Chen, J. Fan, Y. Dong, Y. Song, X. Du, P. Wang, Y. Yang, *Crystal Growth & Design* **2016**, *16*, 5429-5440; c) P. Wu, Y. Liu, Y. Liu, J. Wang, Y. Li, W. Liu, J. Wang, *Inorganic chemistry* **2015**, *54*, 11046-11048; d) J. Zhang, J. Wu, G. Tang, J. Feng, F. Luo, B. Xu, C. Zhang, *Sensors and Actuators B: Chemical* **2018**, *272*, 166-174.
- [15] a) J. Y. Zou, Ling Li, Sheng-Yong You, Yue-Wei Liu, Hong-Min Cui, Jian-Zhong Cui, S.-W. Zhang, *Dalton transactions* **2018**. b) X. Mi, D. Sheng, Y. Yu, Y. Wang, L. Zhao, J. Lu, Y. Li, D. Li, J. Dou, J. Duan, S. Wang, *ACS applied materials & interfaces* **2019**, *11*, 7914-7926; c) X.-M. Meng, Y.-C. Li, K.-R. Huang, J.-Q. Long, L.-S. Cui, *Inorganica Chimica Acta* **2018**, *482*, 284-291.
- [16] T. Kumar, M. Venkateswarulu, B. Das, A. Halder, R. R. Koner, *Dalton transactions* **2019**, *48*, 12382-12385.
- [17] a) L. Xu, Y. Xu, X. Li, Z. Wang, T. Sun, X. Zhang, *Dalton transactions* **2018**, *47*, 16696-16703; b) J. Wang, Q. S. Zhang, W. Dou, A. M. Kirillov, W. S. Liu, C. Xu, C. L. Xu, R. Fang, L. Z. Yang, *Dalton transactions* **2018**, *47*, 465-474.
- [18] a) X.-Z. Song, S.-Y. Song, S.-N. Zhao, Z.-M. Hao, M. Zhu, X. Meng, L.-L. Wu, H.-J. Zhang, *Advanced Functional Materials* **2014**, *24*, 4034-4041; b) F. Zhao, X. Y. Guo, Z. Liu, Y.-Q. Wang, *Dalton transactions* **2018**, *47*,

- 8972-8982 ; c) Z. Q. Liu, Y. Zhao, X. D. Zhang, Y. S. Kang, Q. Y. Lu, M. Azam, S. I. Al-Resayes, W. Y. Sun, *Dalton transactions* **2017**, *46*, 13943-13951.
- [19] a) Y. Su, J. Yu, Y. Li, S. F. Z. Phua, G. Liu, W. Q. Lim, X. Yang, R. Ganguly, C. Dang, C. Yang, Y. Zhao, *Communications Chemistry* **2018**, *1*; b) W. Liu, X. Huang, C. Xu, C. Chen, L. Yang, W. Dou, W. Chen, H. Yang, W. Liu, *Chemistry* **2016**, *22*, 18769-18776.
- [20] a) W. H. Huang, J. Ren, Y. H. Yang, X. M. Li, Q. Wang, N. Jiang, J. Q. Yu, F. Wang, J. Zhang, *Inorganic chemistry* **2019**; b) W. Yang, H. R. Tian, J. P. Li, Y. F. Hui, X. He, J. Li, S. Dang, Z. Xie, Z. M. Sun, *Chemistry* **2016**, *22*, 15451-15457; c) Y. Liu, J. Ma, C. Xu, Y. Yang, M. Xia, H. Jiang, W. Liu, *Dalton transactions* **2018**, *47*, 13543-13549.
- [21] a) R. Fu, S. Hu, X. Wu, *Journal of Materials Chemistry A* **2017**, *5*, 1952-1956; b) C. F. Pereira, F. Figueira, R. F. Mendes, J. Rocha, J. T. Hupp, O. K. Farha, M. M. Q. Simoes, J. P. C. Tome, F. A. A. Paz, *Inorganic chemistry* **2018**, *57*, 3855-3864; c) C. Q. Jiao, M. Sun, F. Liu, Y. N. Zhou, Y. Y. Zhu, Z. G. Sun, D. P. Dong, J. Li, *ACS omega* **2018**, *3*, 16735-16742; d) H. Pan, S. Wang, X. Dao, Y. Ni, *Inorganic chemistry* **2018**, *57*, 1417-1425.
- [22] a) G. T. Wang, J.C. Zhang, Z. Y. Tang, H.-T. Zhou, L. Zhang, R. W. Yang, P. Zou, Y. H. Yu, J. S. Gao, G. F. Hou, *CrystEngComm* **2016**, *18*, 2437-2445; b) G. T. Wang, Z. Y. Tang, H. T. Zhou, P. Zou, H. B. Rao, Y. S. Zhang, G.-F. Hou, *Polyhedron* **2016**, *117*, 259-264.
- [23] G. M. Sheldrick, *Acta crystallographica. Section A, Foundations of crystallography* **2008**, *64*, 112-122.
- [24] a) C. David, C. Jordi, L. Miquel, A. Pere, A. David, A. Santiago, *Journal of the American Chemical Society* **2004**, *126*, 1755-1763; b) M. Pinsky, D. Avnir, *Inorganic chemistry* **1998**, *37*, 5575.
- [25] a) Y.-F. Liu, G.-F. Hou, Y.-H. Yu, P.-F. Yan, J.-Y. Li, G.-M. Li, J.-S. Gao, *Crystal Growth & Design* **2013**, *13*, 3816-3824; b) Y. Zhao, C.-Q. Jiao, Z.-G. Sun, Y.-Y. Zhu, K. Chen, C.-L. Wang, C. Li, M.-J. Zheng, H. Tian, S.-H. Sun, W. Chu, *Crystal Growth & Design* **2012**, *12*, 3191-3199; c) J. Diwu, D. J. Grant, S. Wang, L. Gagliardi, T. E. Albrecht-Schmitt, *Inorganic chemistry* **2012**, *51*, 6906-6915; d) Z. Amghouz, S. García-Granda, J. R. García, A.

Clearfield, R. Valiente, *Crystal Growth & Design* **2011**, *11*, 5289-5297.

- [26] A. L. Spek, *Acta crystallographica. Section D, Biological crystallography* **2009**, *65*, 148-155.
- [27] V. A. Blatov, *IUCr CompComm Newsletter* **2006**, *7*, 4-38.
- [28] K. Binnemans, *Coordination Chemistry Reviews* **2015**, *295*, 1-45.
- [29] P. Mahata, S. K. Mondal, D. K. Singha, P. Majee, *Dalton transactions* **2017**, *46*, 301-328.
- [30] a) L. Li, Q. Chen, Z. Niu, X. Zhou, T. Yang, W. Huang, *Journal of Materials Chemistry C* **2016**, *4*, 1900-1905; b) G. P. Li, G. Liu, Y. Z. Li, L. Hou, Y. Y. Wang, Z. Zhu, *Inorganic chemistry* **2016**, *55*, 3952-3959; c) Q. Tang, S. Liu, Y. Liu, J. Miao, S. Li, L. Zhang, Z. Shi, Z. Zheng, *Inorganic chemistry* **2013**, *52*, 2799-2801; d) C. Yao, Y. Xu, Z. Xia, *Journal of Materials Chemistry C* **2018**, *6*, 4396-4399.
- [31] a) Z. Hao, G. Yang, X. Song, M. Zhu, X. Meng, S. Zhao, S. Song, H. Zhang, *J. Mater. Chem. A* **2014**, *2*, 237-244; b) J. Wang, J. Wang, Y. Li, M. Jiang, L. Zhang, P. Wu, *New Journal of Chemistry* **2016**, *40*, 8600-8606.
- [32] S. Dang, E. Ma, Z.-M. Sun, H. Zhang, *Journal of Materials Chemistry* **2012**, *22*, 16920.
- [33] M. Zheng, H. Tan, Z. Xie, L. Zhang, X. Jing, Z. Sun, *ACS applied materials & interfaces* **2013**, *5*, 1078-1083.
- [34] B. Chen, L. Wang, Y. Xiao, F. R. Fronczek, M. Xue, Y. Cui, G. Qian, *Angewandte Chemie* **2009**, *48*, 500-503.
- [35] Z. Hao, X. Song, M. Zhu, X. Meng, S. Zhao, S. Su, W. Yang, S. Song, H. Zhang, *Journal of Materials Chemistry A* **2013**, *1*, 11043.

Figure Captions

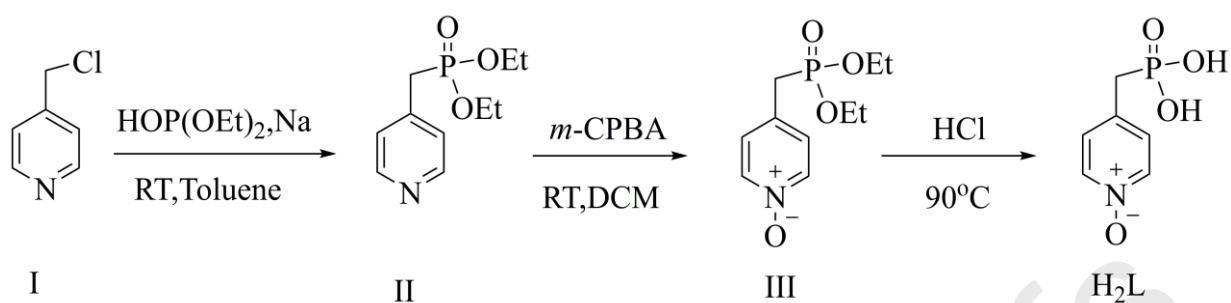
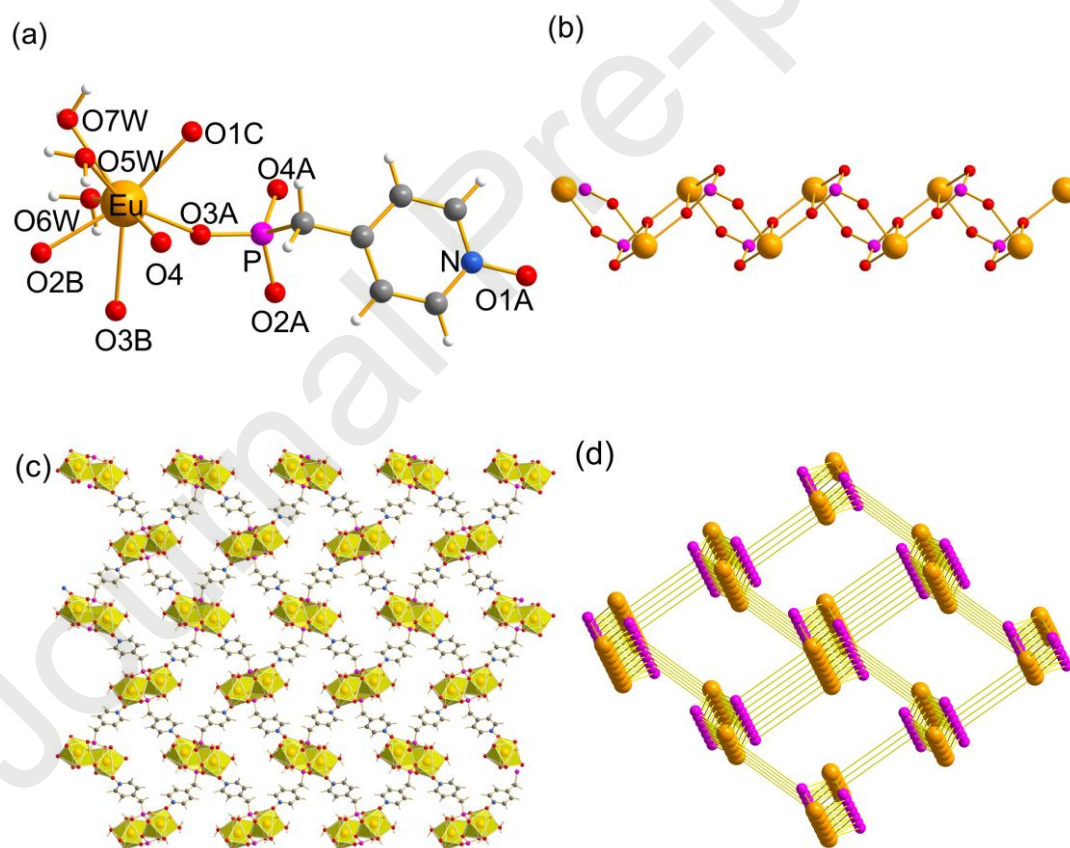
Scheme 1. Synthesis of H₂L.

Figure 1. (a) Coordination environment of Eu^{3+} in **1**; (b) The 1D chain bridged by phosphoric acid; (c) 3D stacked view of **1** along the a-axis; (d) the topology of **1**.

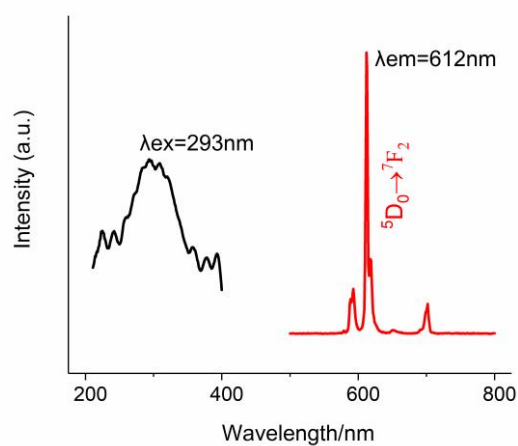


Figure 2. Fluorescence excitation and emission spectra of **1**.

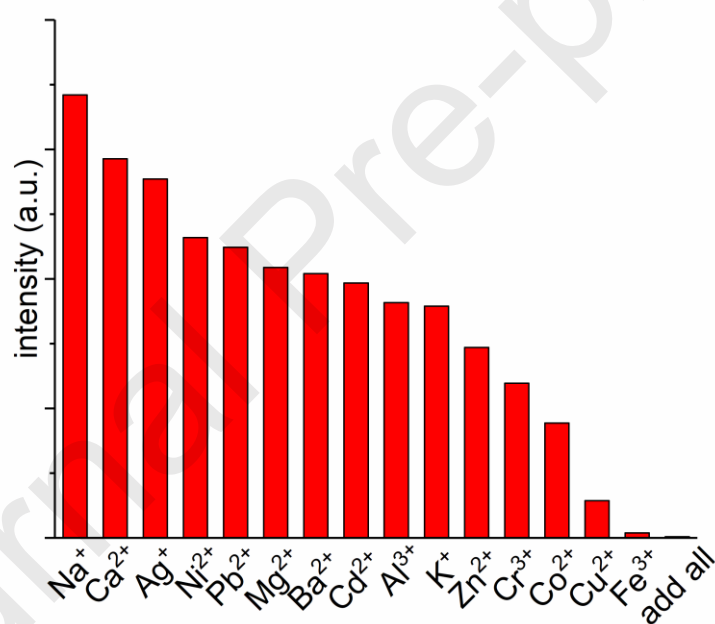


Figure 3. Luminescence intensities of the ${}^5D_0 \rightarrow {}^7F_2$ transition of **1** dispersed in DMF solutions of different metal ions. Excitation wavelength: 280 nm.

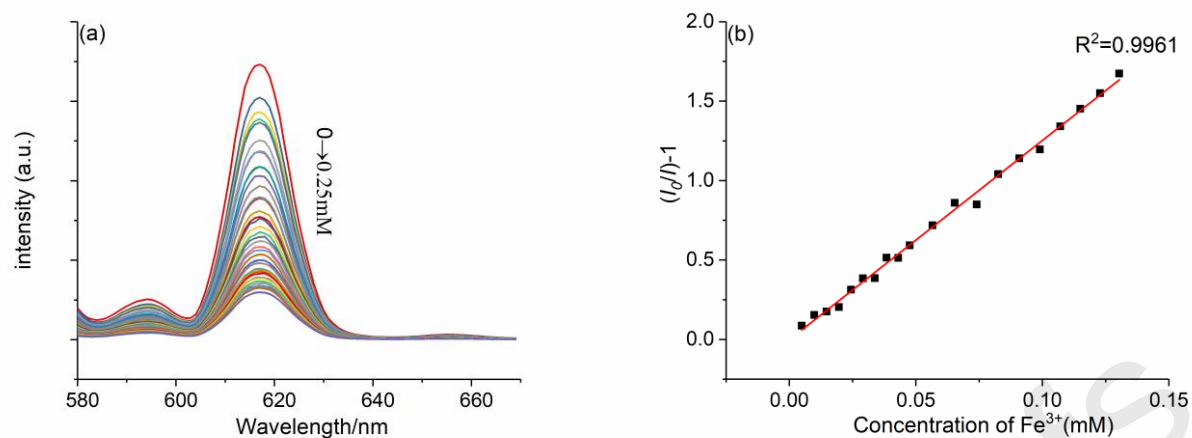


Figure 4. (a) Response of fluorescence emission spectra of **1** to various concentrations of Fe^{3+} ; (b) linear fitting curves of luminescence intensities quenched by Fe^{3+} with different concentrations. Excitation wavelength: 280 nm.

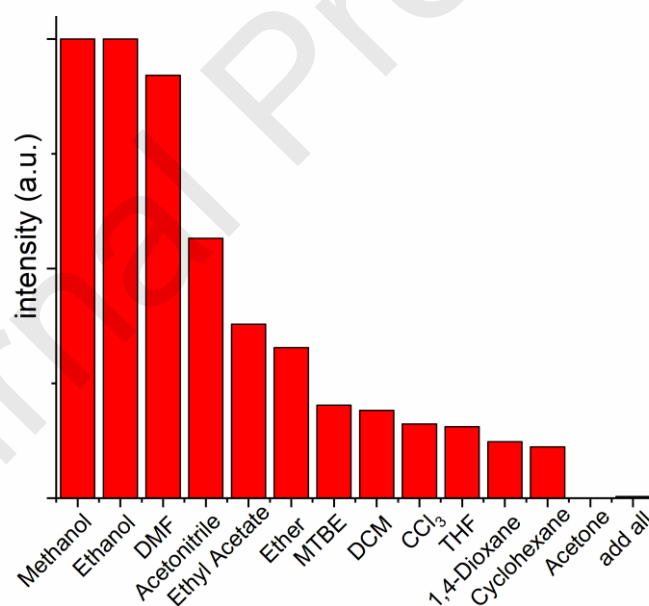


Figure 5. Luminescence intensities of the ${}^5\text{D}_0 \rightarrow {}^7\text{F}_2$ transition of **1** dispersed in different small organic molecules. Excitation wavelength: 280 nm.

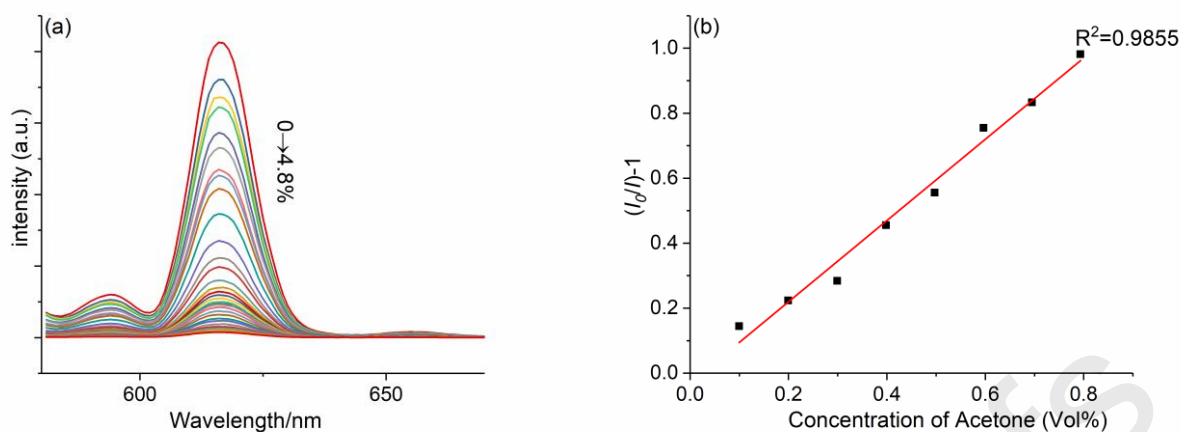


Figure 6. (a) Response of fluorescence emission spectra of **1** to various concentrations of Acetone; (b) linear fitting curves of luminescence intensities quenched by Acetone with different concentrations. Excitation wavelength: 280 nm.

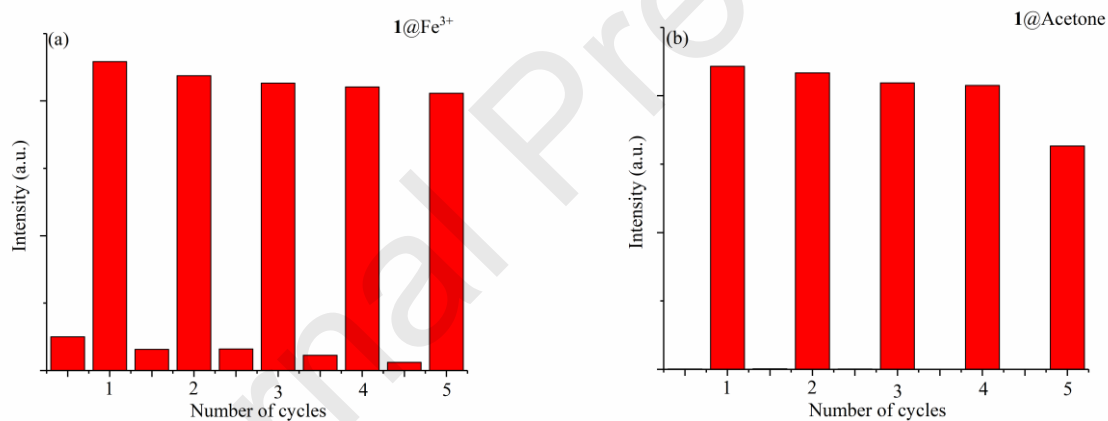
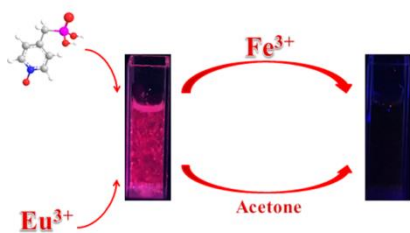


Figure 7. (a) Five cycle tests of **1** towards sensing Fe^{3+} in DMF; (b) Five cycle tests of **1** towards sensing acetone in DMF. Excitation wavelength: 280 nm.

Mandatory graphical abstract

A new Eu-based phosphonate coordination polymer was successfully synthesized by diffusion at room temperature. The obtained coordination polymer can be used as a fluorescent sensor to sensitively and

selectively sense Fe^{3+} and acetone.



Journal Pre-proofs